Effect of Film Thickness on the Far- and Near-field Optical Response of Nanoparticle-on-film Systems

Rachel E. Armstrong*, J.C. van Liempt, and Peter Zijlstra

Eindhoven University of Technology

Department of Applied Physics

Institute for Complex Molecular Systems

Postbus 513, 5600 MB, Eindhoven, The Netherlands

Email: r.e.armstrong@tue.nl

Supplemental Information

I. Gold film thickness by Dektak XT stylus profilometer

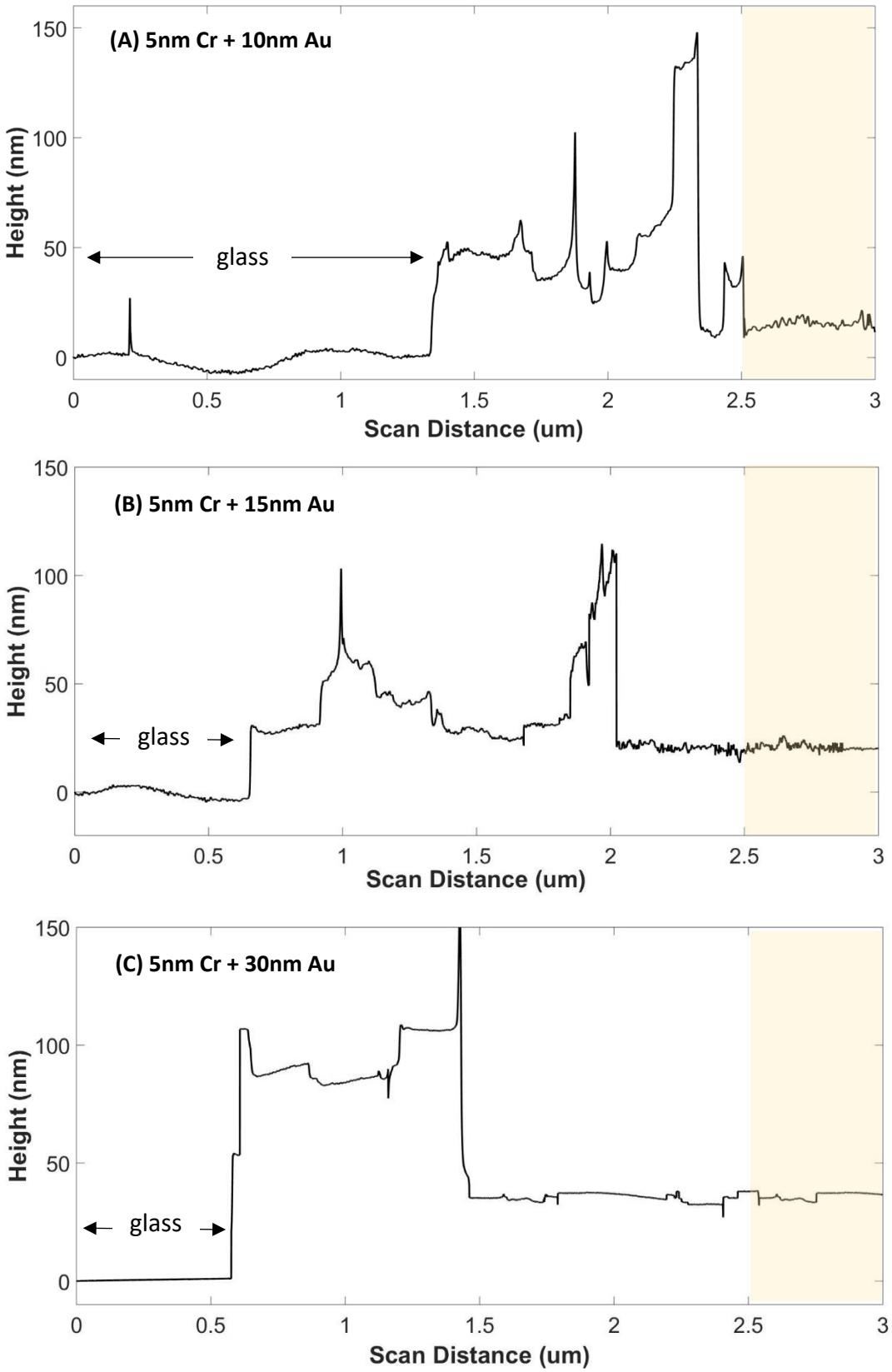

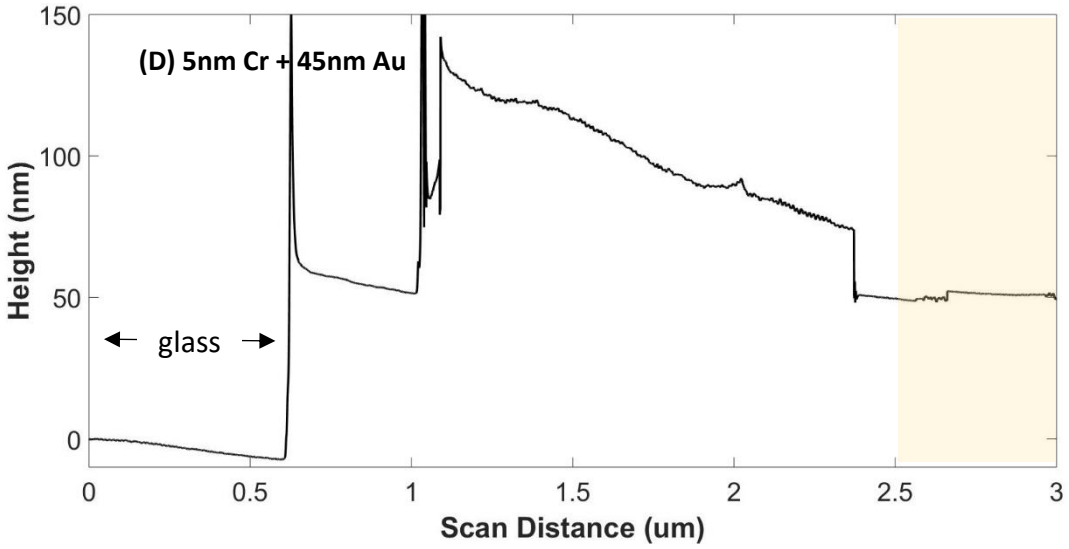

Figure SF1. (A-D) Height profiles across a region transitioning from bare glass to 5nm Cr layer plus gold layer. A 10nm gold layer is shown in (A), 15 nm gold film in (B), 30 nm gold film in (C), and a 45nm gold film in (D). The glass region was blocked by tape during the gold evaporation and removed afterwards to analyze the height profile of the gold layer. The measured section was selected by aligning the needle by eye in the software's camera. Then, the film height determination was calculated by the average height across the final 0.5 μm of the scan (shaded) to avoid the noisy portions that stem from peeling back the tape. Comparisons to other methods by the European discussion group for Nanometrology estimate a std. deviation of ~2nm across step-height thicknesses ranging from 7-800nm for this method of stylus profilometry (1).

II. UV-Vis spectroscopy of gold films

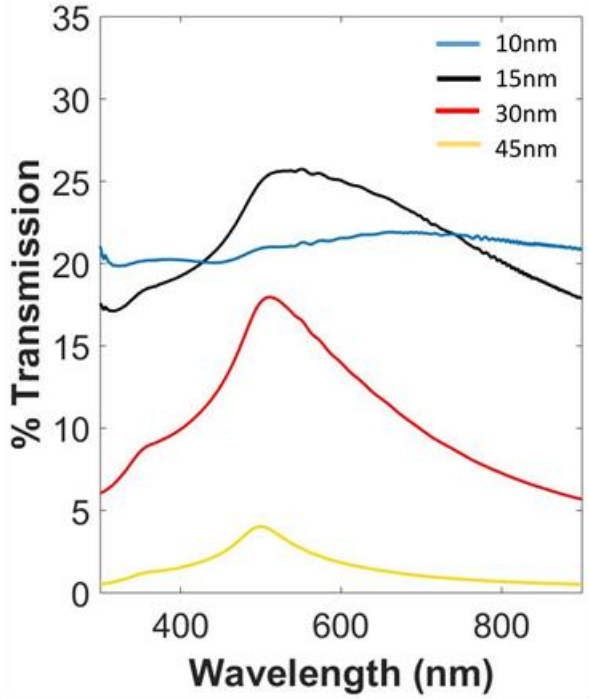

Figure SF2. Percent transmission of the films prepared for this study as measured by UV-Vis spectroscopy. These spectra are in good agreement with previous studies that report a large change in the spectral profile of gold films when thickening from 10 to 15 nm (2-4). The presence of the 5 nm chromium adhesion layer has a much stronger impact on the thinner (<30 nm) films, specifically, a higher optical absorption from 300-400 nm and a broadening of the gold absorption peak (3). We observe near total extinction by gold films of 45 nm thickness, which is expected as films at this thickness begins to behave as a near-perfect mirror.

III. Polymer spacer characterization by ellipsometry

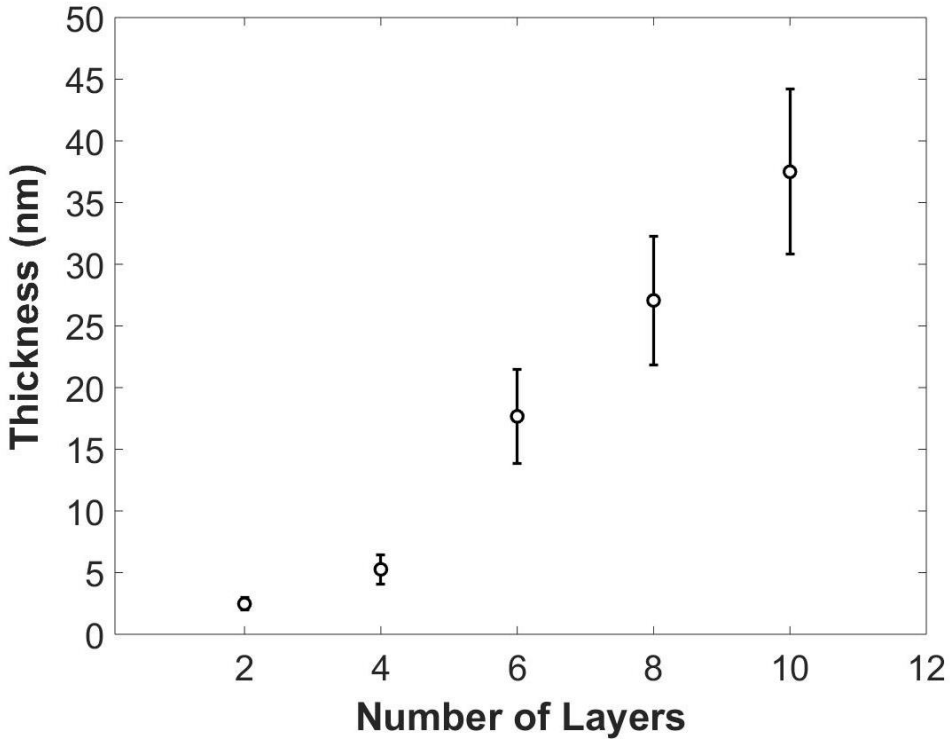

Figure SF3. Polymer spacer thickness calibration by ellipsometry. Each point is the average of three samples and the error bars represent the highest and lowest value of the three. A cauchy fit was applied to extract the thickness. The fit parameters were found to be A= 1.617, B= -0.3087 m^2 , and C= -0.00887 m^4 for the Cauchy equation $n(\lambda) = A + B(\lambda^{-2}) + C(\lambda^{-4})$, where n is the refractive index of the polymer and λ is the incident wavelength.

IV. AFM of gold nanoparticles on the film/polymer surface

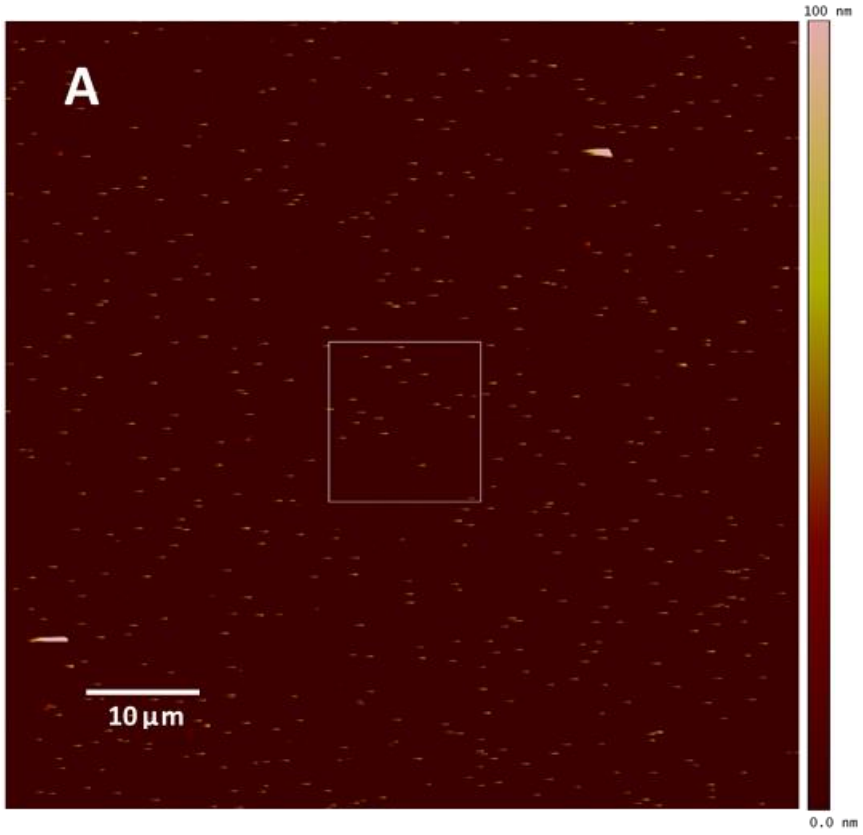

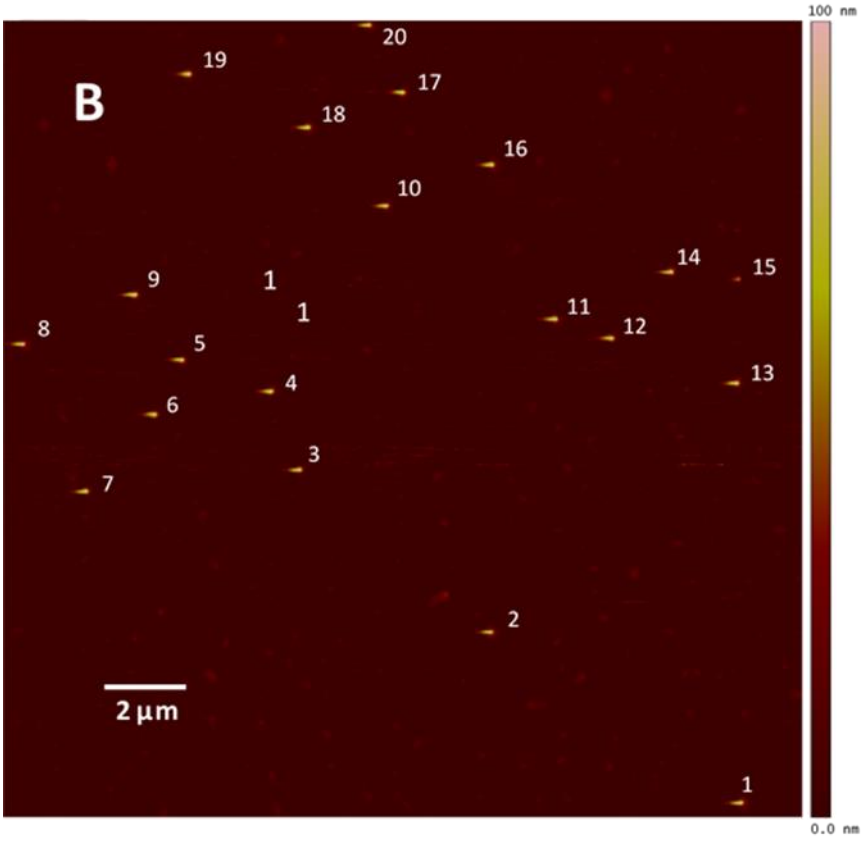

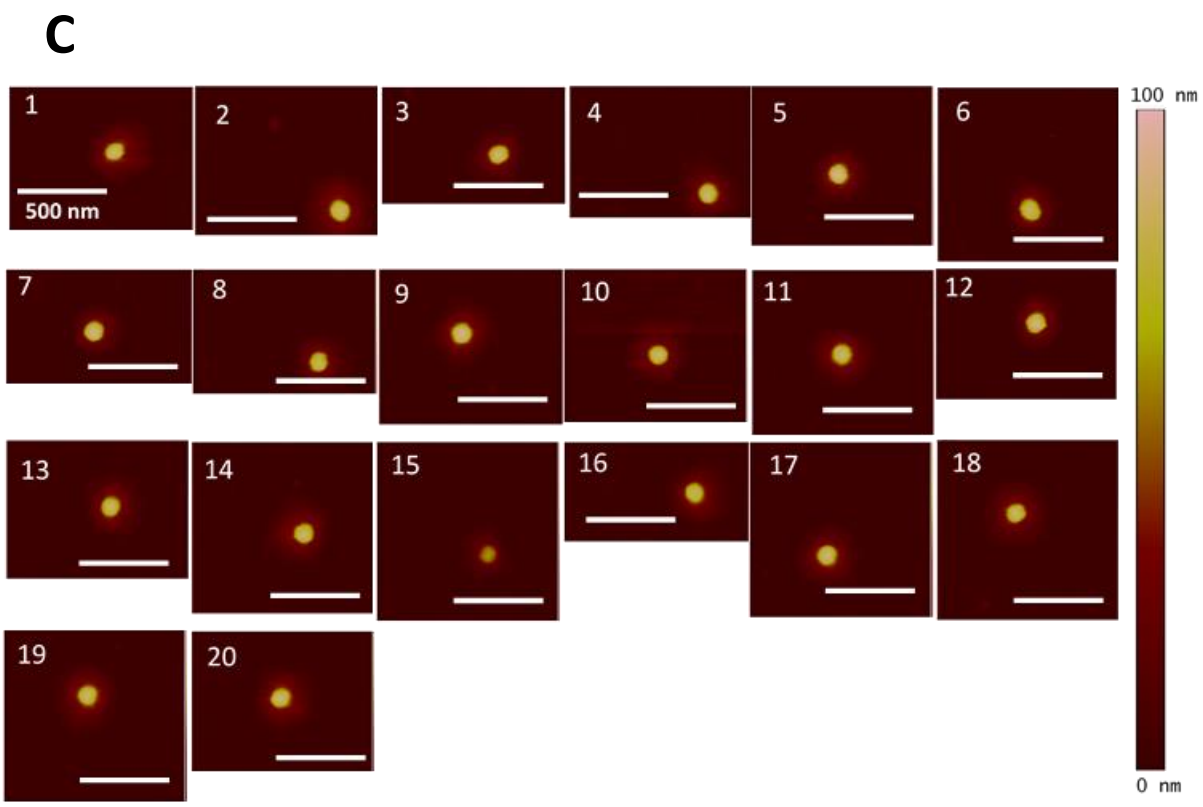

Figure SF4. AFM images of gold nanoparticles spin-coated onto the polymer/gold film surface. Densities across the sample vary and here a high density (20 particles/400µm^2) was chosen to obtain as much single particle information as possible. (A) Scan area of 100µm x 100µm. A zoomed-in image of the center square is shown in B. (B) The 20µm x 20µm square area denoted in A. Nanoparticles "streaks" observed in A and B are a result of the faster scan rate required for larger areas. (C) Individual particle images of the 20 nanoparticles observed in B. Nearly all nanoparticles are 95-105nm in width and height (except for #15), and are spherical, as was confirmed previously by TEM (main text Figure 1B). No dimers are observed in this field of view, ensuring the spin-coating procedure does not induce clustering.

V. Calculated far-field spectra dependence on the angle of incidence

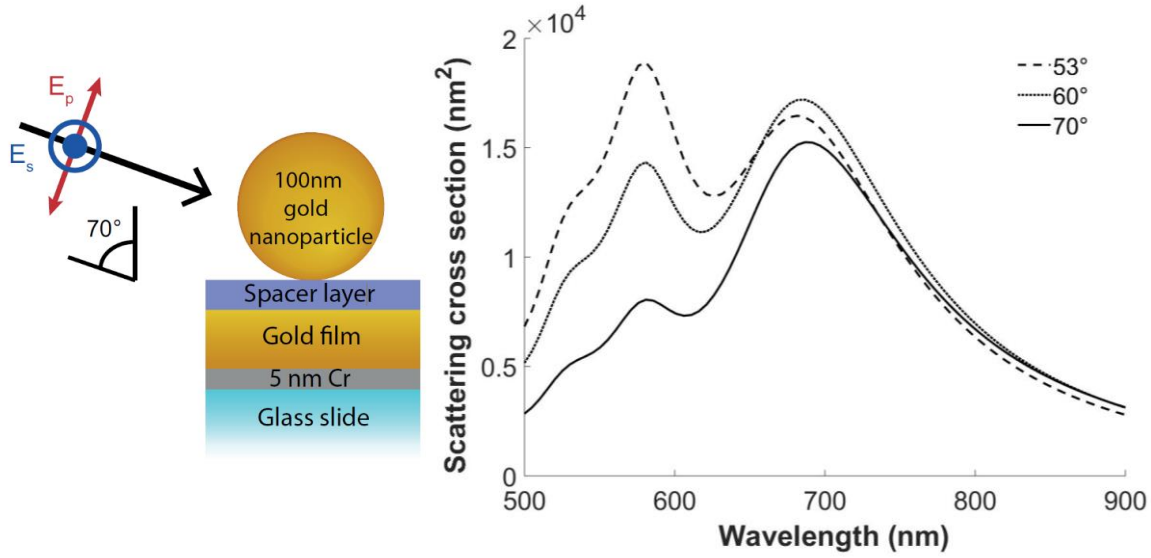

Figure SF5. (Left) Geometry constructed in the BEM toolbox for far-field simulations. (Right) BEM-calculated spectra of a gold nanoparticle on a 45nm film (5 nm gap spacing), where the angle of incidence is 53° (dashed line), 60° (dotted line), and 70° (solid line). The dark-field condenser likely provides of a mixture of incident angles. We compare experimental data only to the spectra calculated with an incident angle of 70° because of the similar prominence of the red-shifted vertical antenna mode observed experimentally.

VI. Gold nanoparticle spectra on glass

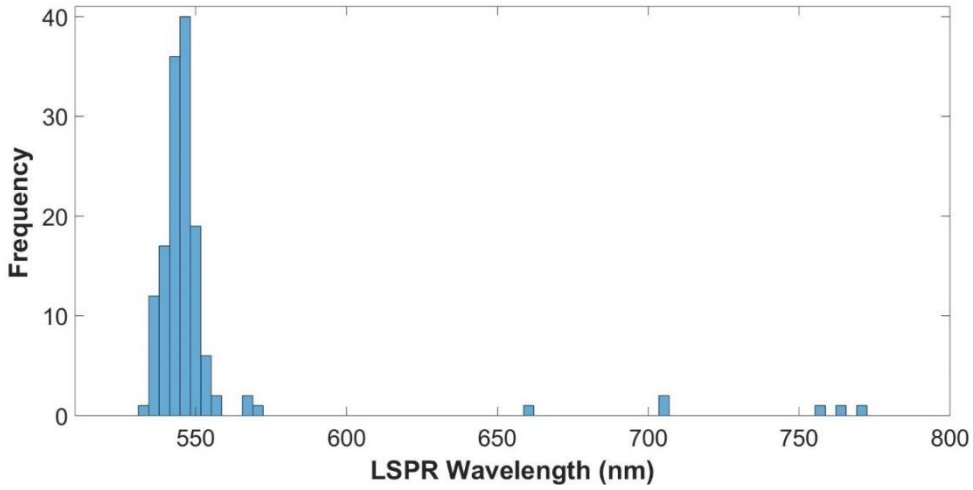

Figure SF6. Histogram of LSPR wavelengths of 100nm gold nanoparticles spin-coated onto a glass microscope slide and measured via hyperspectral microscopy in the described setup. The sole LSPR intensity at 540nm is expected as the nanoparticles are not coupled to a gold film and therefore exhibit unaffected vertical antenna/transverse plasmons. A few occurrences of plasmon resonances >600 nm indicate a low fraction of aggregates in the sample.

VII. Calculated effect of Cr in the far-field spectra

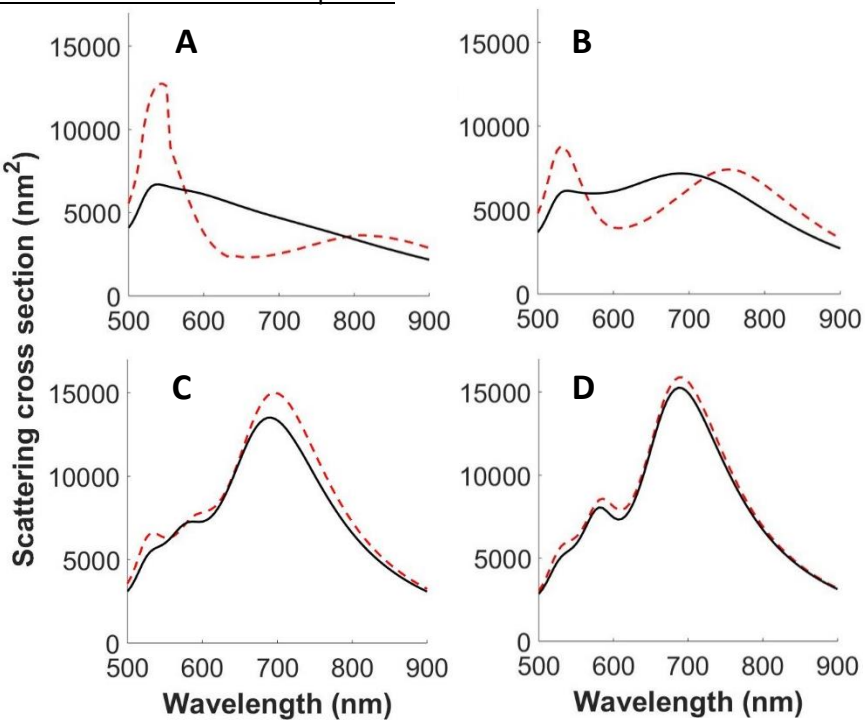

Figure SF7. Calculated far-field spectra of a 100 nm gold nanoparticle located 5 nm above a gold film. Black lines represent the samples where a 5 nm chromium layer beneath the gold film is considered, and red lines represent the simulated spectra without chromium. Each graph is a different gold film thickness – (A) 10 nm, (B) 15 nm, (C) 30 nm, and (D) 45 nm.

VIII. AFM surface roughness analysis for film thicknesses of 10 nm, 15 nm, 30 nm, and 45 nm

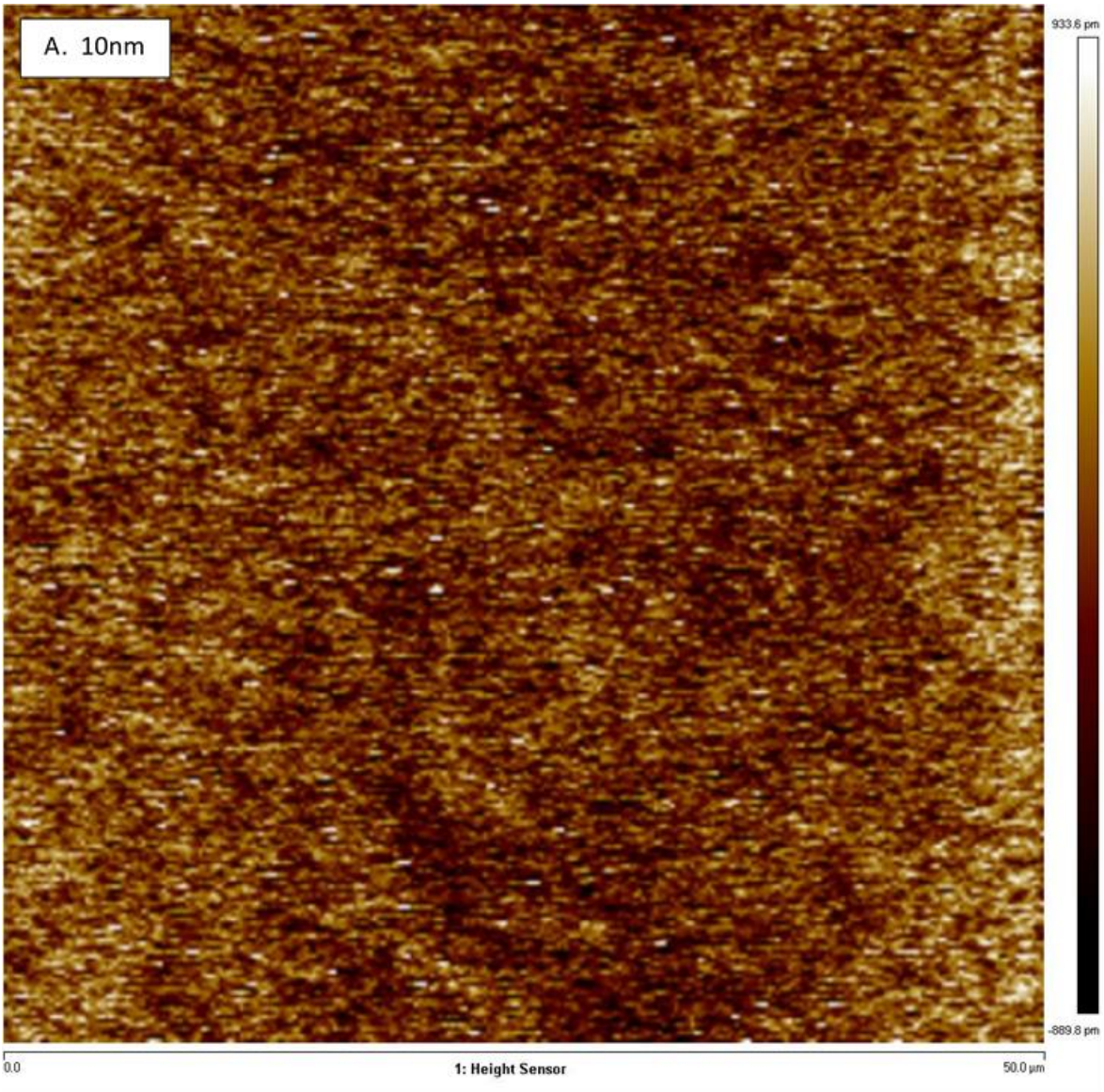

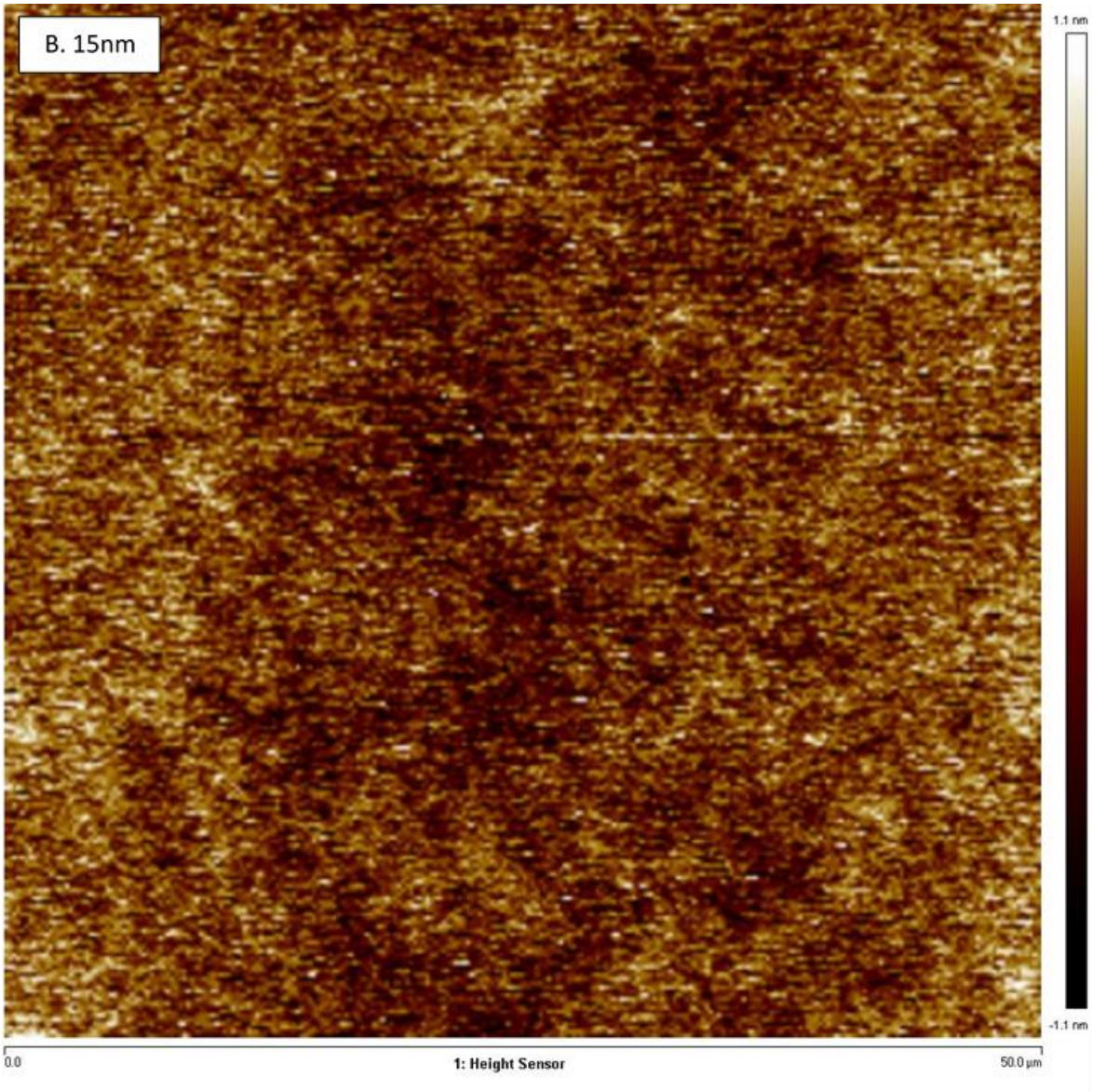
B. 15nm
1.1 nm
-1.1 nm
0.0
1: Height Sensor
50.0 µm

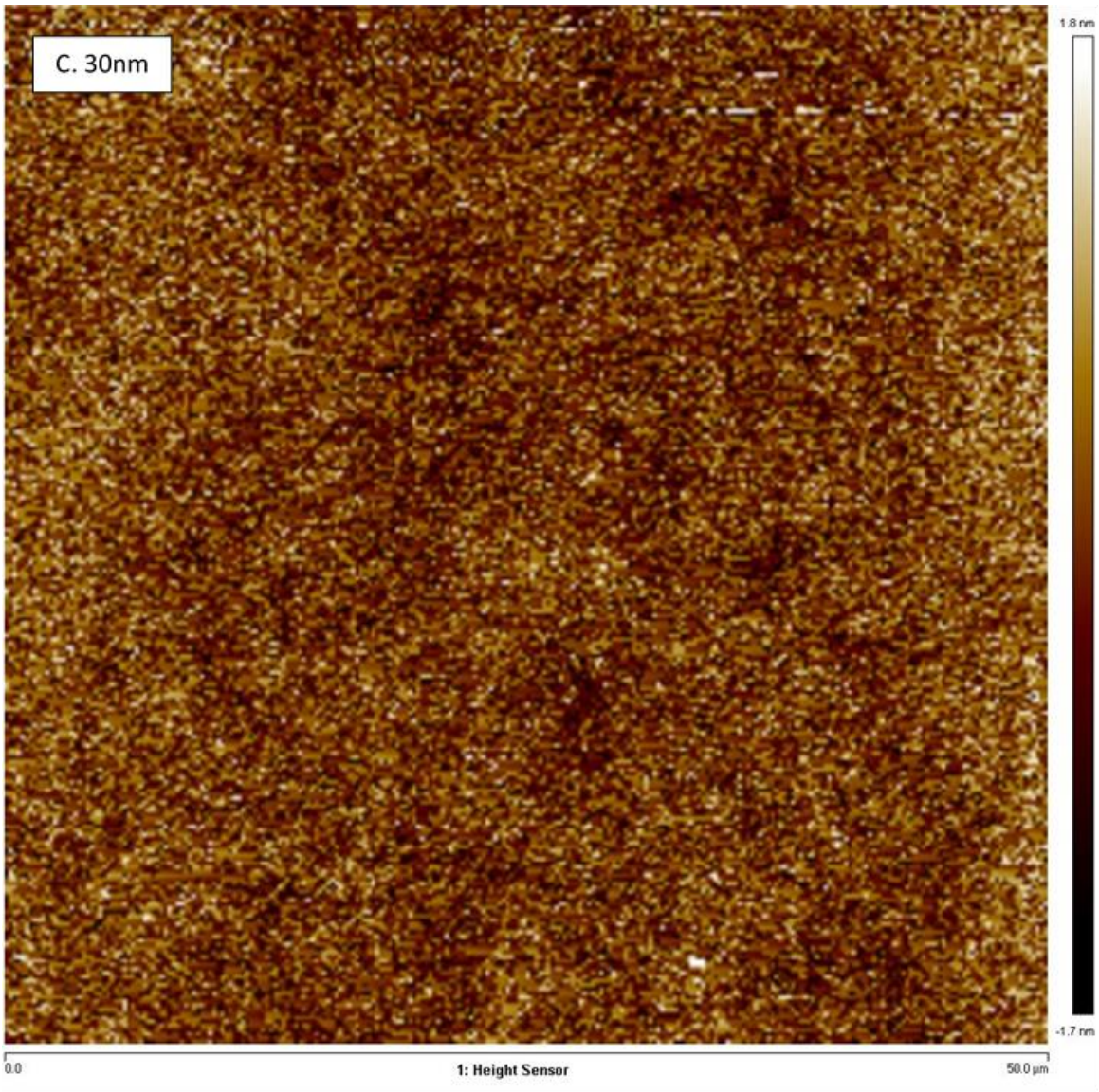
C. 30nm
1.8 nm
-1.7 nm
0.0
1: Height Sensor
50.0 µm

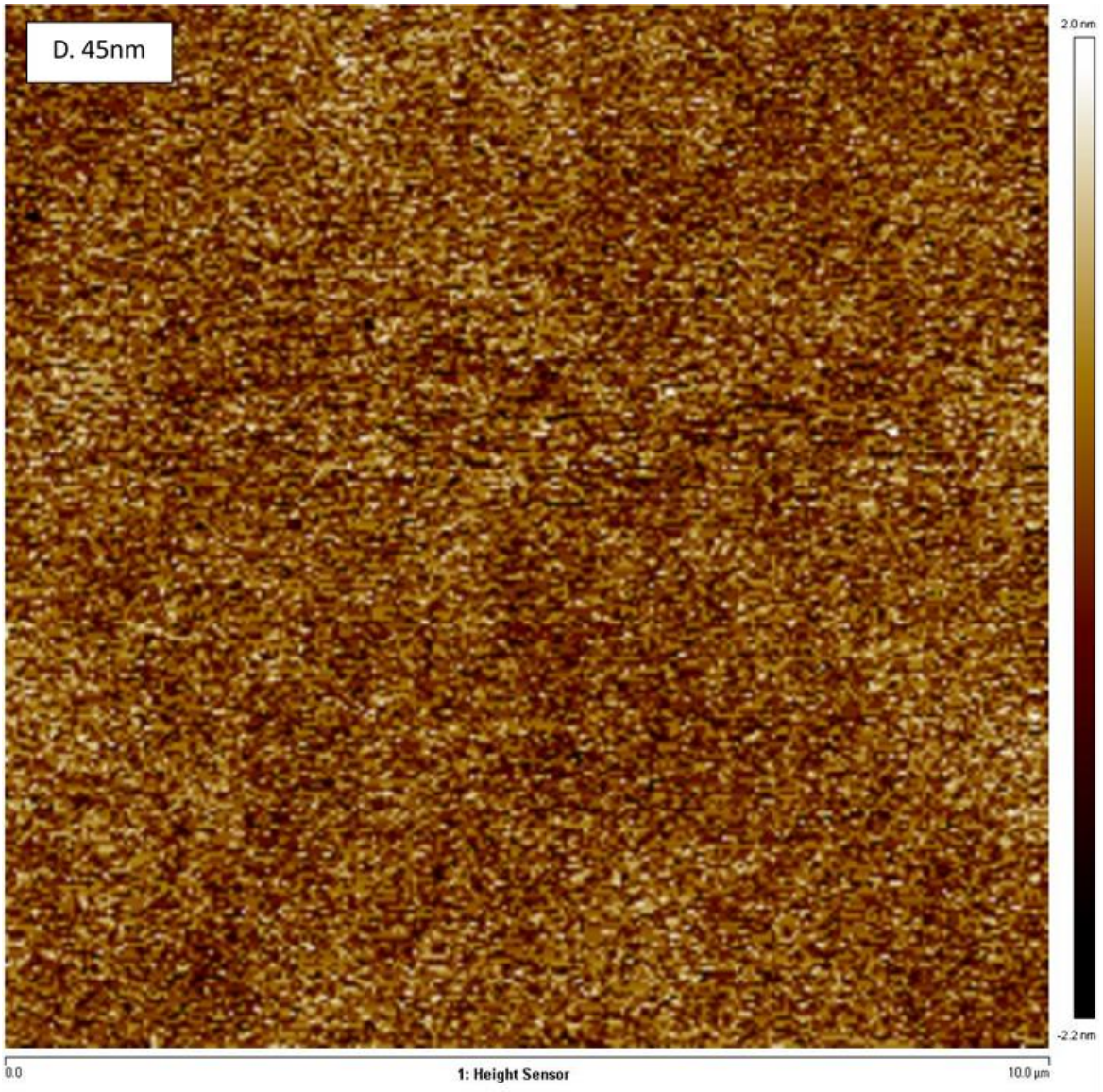

Figure SF8. (A-D) AFM height analysis images of a 10nm gold film (A), 15nm gold film (B), 30nm gold film (C), and 45 nm gold film (D) prior to polymer deposition. Note that the color bar scales vary slightly for each image. Surface roughness scan data (R_q and R_a) for multiple scans per sample are presented in Table S1.

Table S1. AFM Surface Roughness Analysis Data			
Film Thickness	Scan size (μm)	R_q (nm)	R_a (nm)
45nm	50	0.489	0.385
	50	0.559	0.388
	50	0.323	0.256
	50	0.378	0.27
30nm	50	0.484	0.385
	50	0.48	0.382
	50	0.484	0.385
	50	0.484	0.384
	50	0.324	0.257
	50	0.332	0.263
15nm	50	0.492	0.388
	50	0.461	0.363
	50	0.354	0.28
	50	0.294	0.231
	50	0.311	0.245
	50	0.293	0.23
	50	0.313	0.248
	50	0.282	0.221
	50	0.45	0.351
	50	0.439	0.344
	50	0.427	0.322
	50	0.426	0.323
10nm	50	0.243	0.191
	50	0.24	0.188
	50	1.14	0.367
	50	0.41	0.319
	50	0.248	0.194
	50	0.237	0.186
	50	0.584	0.415
	50	0.506	0.382

IX. Calculated far-field spectra as a function of gap spacing

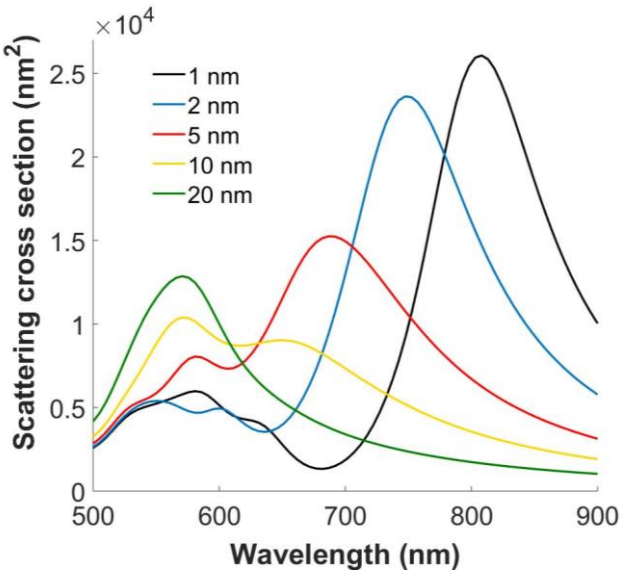

Figure SF9. BEM calculated far-field spectra of a gold nanoparticle at various gap spacings above a 45 nm gold film.

X. Calculated far-field spectra with Palik vs. Johnson & Christy gold constants

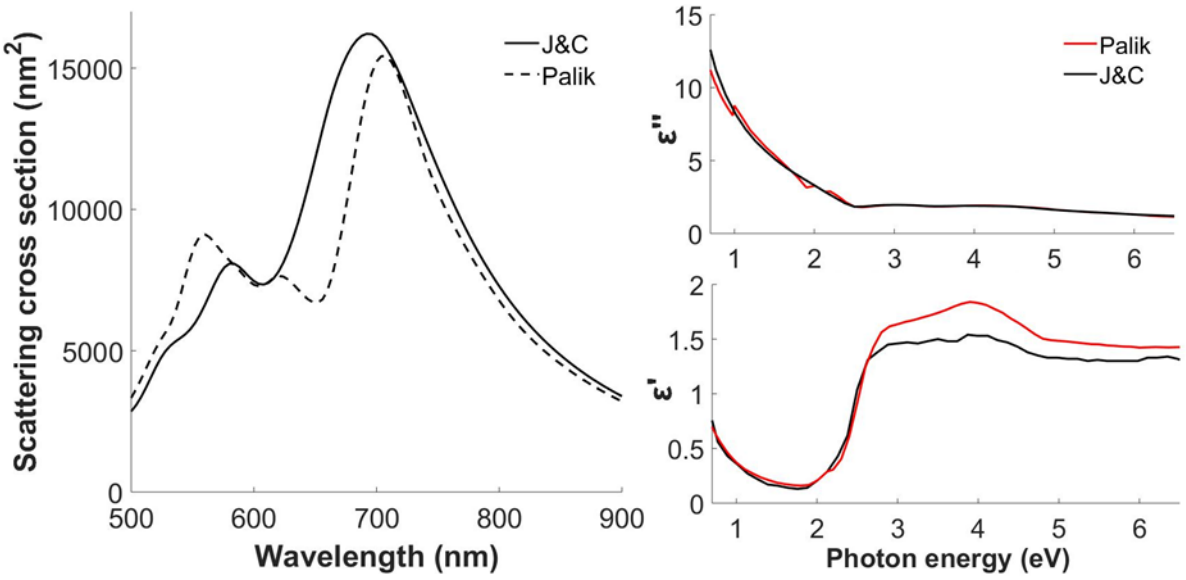

Figure SF10. (Left) BEM-simulated far-field spectra of a gold nanoparticle on a 45 nm film (5 nm gap spacing) using gold optical constants reported by Johnson & Christy (solid line) and those reported by Palik (dashed line). (Right) Real (bottom) and imaginary (top) components of the gold dielectric function as reported by Johnson & Christy (black) and Palik (red). Subtle differences in the real parts of the gold refractive index are capable of producing significant differences in the calculated vertical antenna mode linewidth and the intensities of the various plasmon modes.

XI. Calculated vertical antenna mode as a function of gap spacing

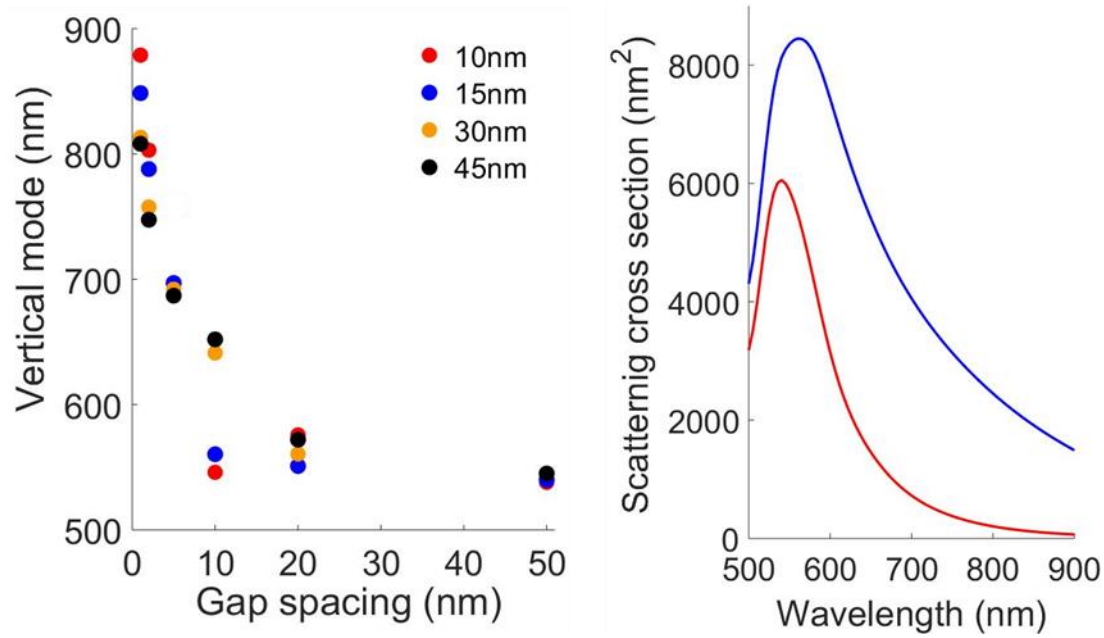

Figure SF11. (Left) BEM-calculated vertical antenna wavelength as a function of gap spacing for each film thickness. Note: The 5nm gap spacing for the 10nm film thickness is not shown as no clear vertical plasmon mode is apparent. (Right) 10nm (red) and 15nm (blue) far-field spectrum at a 10nm gap spacing. The 10nm and 15nm film are artificially blue-shifted here, as the vertical plasmon is strongly overlapped with the transverse/quadrupole modes. This results in a single, broadened peak, making an accurate multi-Lorentzian fit difficult. Therefore the center of the broadened peak is given as the plasmon resonance for these film thicknesses, though the actual plasmon is more likely to be a red-shifted shoulder off the peak.

References

1. Koenders, L.; Bergmans, R.; Garnaes, J.; Haycocks, J.; Korolev, N.; Kurosawa, T.; Meli, F.; Park, B. C.; Peng, G. S.; Picotto, G. B., Comparison on Nanometrology: Nano 2-Step height. *Metrologia* **2003,** *40* (1A), 04001.

2. Lozanova, V.; Lalova, A.; Soserov, L.; Todorov, R., Optical and electrical properties of very thin chromium films for optoelectronic devices. *Journal of Physics: Conference Series* **2014,** *514*, 012003.

3. Siegel, J.; Lyutakov, O.; Rybka, V.; Kolska, Z.; Svorcik, V., Properties of gold nanostructures sputtered on glass. *Nanoscale Research Letters* **2011,** *6* (1), 96.

4. Axelevitch, A.; Apter, B.; Golan, G., Simulation and experimental investigation of optical transparency in gold island films. *Optics Express* **2013,** *21* (4), 4126-4138.